International Journal of Pharmaceutics 508 (2016) 71–82

Contents lists available at ScienceDirect

International Journal of Pharmaceutics

journal homepage: www.elsevier.com/locate/ijpharm

Monitoring the recrystallisation of amorphous xylitol using Raman spectroscopy and wide-angle X-ray scattering

Emmi Palomäki[a,*], Patrik Ahvenainen[b], Henrik Ehlers[a], Kirsi Svedström[b], Simo Huotari[b], Jouko Yliruusi[a]

[a] Faculty of Pharmacy, P.O. Box 56, FI-00014 University of Helsinki, Finland
[b] Department of Physics, P.O. Box 64, FI-00014 University of Helsinki, Finland

ARTICLE INFO

Article history:
Received 29 January 2016
Received in revised form 22 April 2016
Accepted 27 April 2016
Available online 7 May 2016

Chemical compounds studied in this article:
Xylitol (PubChem CID 6912)
Silica (PubMed CID 24261)
Ibuprofen (PubChem CID 3672)
Indomethacin (PubChem CID 3715)

Keywords:
Amorphous
Crystallization
Raman spectrometry
Wide-angle X-ray scattering
Xylitol
Non-ordered mesoporous silica

ABSTRACT

In this paper we present a fast model system for monitoring the recrystallization of quench-cooled amorphous xylitol using Raman spectroscopy and wide-angle X-ray scattering. The use of these two methods enables comparison between surface and bulk crystallization. Non-ordered mesoporous silica micro-particles were added to the system in order to alter the rate of crystallization of the amorphous xylitol. Raman measurements showed that adding silica to the system increased the rate of surface crystallization, while X-ray measurements showed that the rate of bulk crystallization decreased. Using this model system it is possible to measure fast changes, which occur in minutes or within a few hours. Raman-spectroscopy and wide-angle X-ray scattering were found to be complementary techniques when assessing surface and bulk crystallization of amorphous xylitol.

1. Introduction

Today, poor aqueous solubility is a common problem when developing new drug products. There are several approaches to deal with solubility issues, such as formation of salts or prodrugs, reducing the particle size or rendering the drug into a disordered state (Hancock and Zografi, 1997; Yu, 2001). Amorphous substances have a solubility superior to their crystalline counterparts due to their higher levels of molecular disorder, free energy and molecular mobility. The beneficial properties of amorphous drug substances are counterweighted by their inherent physical instability and tendency to undergo solid-state changes to reach the most stable crystal form.

Recrystallization from the amorphous state can take anything from hours to years. Considerable effort and resources have been invested in trying to achieve amorphous formulations with high enough stability to ensure sufficient physical stability of the active pharmaceutical ingredient throughout the shelf life of the final product. Still, a complete understanding of the crystallization of amorphous solids has not been achieved (Laitinen et al., 2013; Bhugra and Pikal, 2008). Typical stability studies of pharmaceuticals take several months to complete, and in order to facilitate the development of drug products to the market there is a need to be able to rapidly screen the physical stability challenges of amorphous drugs.

It has been shown that the surface crystallization is more rapid than bulk crystallization in amorphous glasses aged below their glass transition temperature (Zhu et al., 2010, 2008; Wu et al., 2007; Wu and Yu, 2006; Yu, 2016). The reason for this can not only be found in the higher molecular mobility of surface molecules compared to bulk molecules, but also in the more pronounced structural relaxation of the surface as compared to the bulk (Hasegawa et al., 2009). When the temperature exceeds the glass transition temperature, the viscosity of the sample decreases, and surface diffusion of molecules is disturbed by viscous flow of the material (Yu, 2016). This interrupts surface crystal growth, and as bulk diffusion is simultaneously promoted the difference between

* Corresponding author at: Division of Pharmaceutical Chemistry and Technology, Faculty of Pharmacy, University of Helsinki, P.O. Box 56 (Viikinkaari 5E), FIN-00014 University of Helsinki, Finland.
E-mail address: emmi.palomaki@helsinki.fi (E. Palomäki).

http://dx.doi.org/10.1016/j.ijpharm.2016.04.074
0378-5173/

the rate of surface and bulk crystallization is expected to become smaller.

Raman spectroscopy is a method commonly used to identify amorphous systems and quantify the amount of crystalline content (Chieng et al., 2011; Strachan et al., 2007). The method provides chemical information of the investigated molecules, and in addition Raman spectroscopy also provides information on inter-molecular interactions, which enables quantifying different solid states of substances. Crystalline content in amorphous samples has been detected down to 1% using Raman spectroscopy (Strachan et al., 2007). Raman spectroscopy is non-invasive, non-destructive, rapid and requires no sample preparation (Chieng et al., 2011), which makes it ideal for real-time monitoring of solid-state changes in pharmaceutical systems.

Powder X-ray diffraction is the most frequently used technique in solid-state analysis, and it is often combined with a spectroscopic method for complementary information (Chieng et al., 2011). Wide-angle X-ray scattering has been used to study the crystal structure of pharmaceutically active substances, excipients and drug products (Dong and Boyd, 2011) and is capable of detecting crystalline content in amorphous systems in amounts comparable to Raman spectroscopy (Paudel et al., 2015). It does not provide chemical information on the sample, but readily provides information on the structure of the studied material, and is able to distinguish molecularly ordered and disordered material (Chieng et al., 2011). In analysis of amorphous systems, WAXS is an indirect method, since it detects lack of order rather than disorder.

In the present study, the crystallization rate of amorphous xylitol was studied. Xylitol is a crystalline pentitole with only one reported stable polymorphic form (Carson et al., 1943; Diogo et al., 2007). Curiously enough, xylitol is an example of a substance with a polymorphic form going extinct, since the stable orthorhombic form has completely superseded over the metastable monoclinic form (Dunitz and Bernstein, 1995). Xylitol has a relatively low glass transition temperature of −24 °C (Talja and Roos, 2001), and it recrystallizes readily in room temperature. To alter the rate of crystallization, non-ordered mesoporous silica (Syloid 244FP) was added to the system in the present study. According to the manufacturer, Syloid 244FP has large surface area of 350 m^2/g, pore size of 15–20 nm and pore volume of 1.6 ml/g. It has previously been shown to increase the solubility of drug substances by allowing them to maintain an amorphous state by confinement in pores and molecular level interaction between the carrier particles and drug substance (Kinnari et al., 2011; Limnell et al., 2011).

The aim of the present study was to investigate whether xylitol can be used as a model substance to study rapid solid-state changes. Furthermore, the study set out to see whether Raman spectroscopy and wide-angle X-ray scattering could be used in studying the recrystallization of amorphous xylitol. The crystallinity and crystallization rate results from Raman measurements were compared with the wide-angle X-ray scattering results.

2. Materials and methods

2.1. Sample preparation

In the present study crystalline xylitol (University Pharmacy, Helsinki, Finland) was used as a model substance. Non-ordered mesoporous silica (Syloid 244FP, Grace GmbH & Co., KG, Germany) was used to modify the crystallization rate of amorphous xylitol. The substances were kept in a zero-humidity desiccator for a minimum of two weeks prior to the experiments. Amorphous xylitol was prepared by melting the crystalline powder on a hot plate set at 180 °C, which is well above the melting point of xylitol (92–96 °C) but clearly below its boiling point (215–217 °C). The melt was quench-cooled in liquid nitrogen and roughly ground while submerged in liquid nitrogen. In samples comprised of xylitol and 10% (m/m) of silica, Syloid 244FP was added to the melt and thoroughly mixed prior to quench cooling and grinding as described above. The amount of sample was 1.35 g in both cases. The liquid nitrogen-sample suspension was transferred into a sample holder and the liquid nitrogen was left to evaporate, and, upon complete evaporation, the solid samples were enclosed between two sheets of 6 μm thick Mylar film in order to insulate them from ambient humidity (Fig. 1). To avoid exposure to atmospheric moisture and oxygen, all the steps of the sample preparation following melting and mixing were performed in a dry nitrogen atmosphere. The final samples had a thickness of 2 mm and a diameter of 15 mm. The lag-time between complete evaporation of the liquid nitrogen and initiation of Raman and wide-angle X-ray scattering measurements was no more than 4 min in all experiments. The sample holder was designed to accommodate both Raman and X-ray measurements. The ibuprofen (Boots Pharmaceuticals, UK) and ϒ-indomethacin (Orion

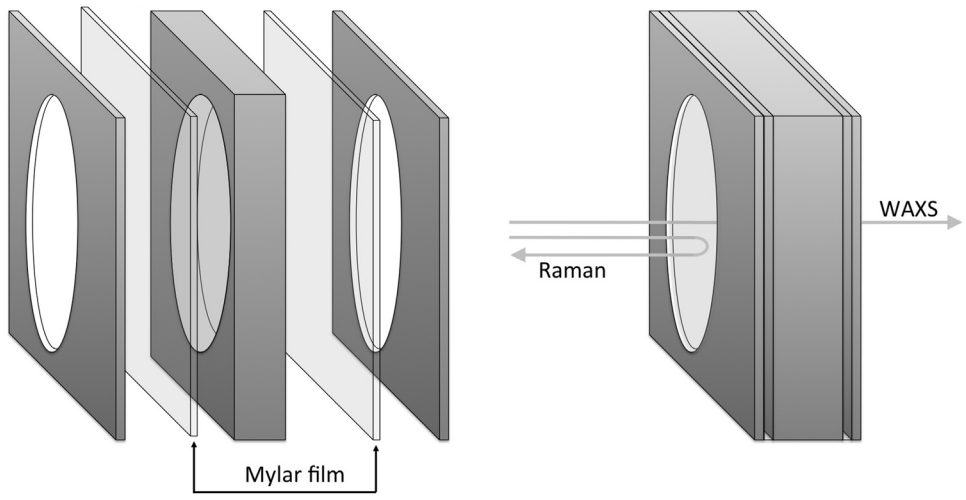

Fig. 1. Sample holder. The 2 mm thick sample (ø 15 mm) is enclosed between two sheets of 6 μm thick Mylar film. Raman-spectroscopy is performed using backscattering geometry and wide angle X-ray scattering is measured with perpendicular transmission geometry.

Pharma, Espoo Finland) used in the penetration depth studies were used as received.

2.2. Solid-state analysis

2.2.1. Raman spectroscopy

The recrystallization of amorphous samples was measured using Raman spectroscopy. The Raman spectra were collected using a Raman RXN1-PhAT-785-D spectrometer (Kaiser, USA) equipped with a PhAt system probe head (Kaiser optical systems, Inc., USA). A 20-mW laser source at 785 nm was used (Raman RXN1-PhAT-785-D, Kaiser aerospace & electronics company, USA). The used spectrometer differs from confocal Raman spectrometry by having a less powerful laser source, which saves the sample from heating. Offset-signals were detected to allow better detection of crystallinity of inhomogeneous sample. One measurement consists of three averaged spectra.

In the present study, the Raman spectrometer laser covers a relatively large area (6 mm in diameter). This minimizes the spectrometer's sensitivity to the exact positioning or the possible inhomogeneity of the sample (Johansson et al., 2005; Paudel et al., 2015). Additionally, the used laser power is relatively small, which reduces the heat load of the sample. Collecting also spatially offset scattering allows deeper detection into sample, since photons generated in the bulk of the sample migrate laterally before emission from the sample (Paudel et al., 2015; Matousek et al., 2005).

The Raman shift recorded was between 100 cm^{-1} and 1920 cm^{-1}, but only Raman shifts between 200 cm^{-1} and 1800 cm^{-1} were used because of inaccuracy in the edges of the Raman shift area. The measurement has an integration time of 2 s and one measurement was the result of three averaged scans. During the recrystallization experiments spectra were collected in ambient conditions with 1-min intervals for 6 h. During the Raman measurements the ambient relative humidity was between 21 and 36% and the ambient temperature between 20.1 and 21.6 °C. In addition, recrystallization was performed in an elevated temperature of 28.5–29.5 °C and relative humidity of 19–25% corresponding to the conditions of the WAXS experiments. In these experiments Raman spectra were collected with 5-min intervals as described above. All recrystallization experiments were performed in triplicate.

Samples of xylitol and xylitol-syloid dispersions were prepared for visual inspection with a microscope. In addition, samples from the final product were placed on an object glass, molten onto the glass and quench cooled in liquid nitrogen before visual inspection using a microscope.

2.2.2. Spectral pretreatment and partial least squares modeling

The spectra were subjected to different combinations of preparations (Fig. 2). The spectra were treated using baseline correction, Savitzky-Golay-smoothing, Standard Normal Variate (SNV), Multiplicative Scatter Correction (MSC), and 1st and 2nd derivatives were constructed. All spectral pretreatment, excluding MSC were performed using MATLAB (MatLab R2014b, MathWorks Inc., Natick, Massachusetts, The United States). The baseline corrections were done with the function msbackadj with a windowsize and stepsize of 25. MSC was done using SimcaP 10.5 (Umetrics AB, Umeå, Sweden).

Reference samples with varying amorphous-crystalline ratios were prepared by adding known amounts of crystalline xylitol into the amorphous xylitol – liquid nitrogen suspension. The reference samples did not contain silica. The amounts of crystalline xylitol in the reference samples were 0 (n = 5), 10 (n = 3), 25 (n = 3), 40 (n = 3), 50 (n = 5), 60 (n = 3), 75 (n = 3), 90 (n = 3) and 100% (n = 5). All individual reference samples were measured in three times.

The xylitol spectra from samples with known amounts of crystalline content were used as reference spectra in the partial least squares (PLS) modeling. Raman shifts of 835.2–1145.4 cm^{-1} were used, which cover most of the strong and mild characteristic peaks in the spectrum and are relatively mildly affected by fluorescence. The choice of the Raman shift area was based on the

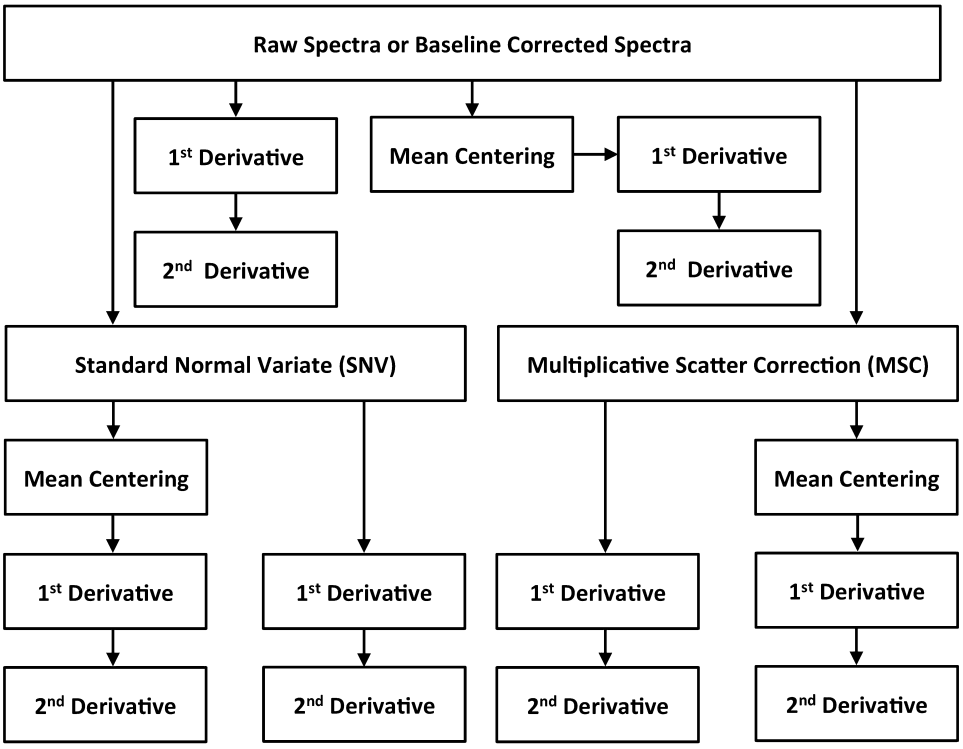

Fig. 2. Pretreatment flow chart of Raman spectra.

peaks growing during crystallization and the characteristic spectral features described by de Veij et al. (2009). The selected range covers the in-phase ν(CCO) stretching vibration at 872 cm^{-1} and a group of peaks in the region between 1000 and 1150 cm^{-1} representing the out-of-phase ν(CCO) stretching vibration. The correlation coefficient R^2 and the predictive strength Q^2 were used to evaluate the PLS-models.

2.2.3. Penetration depth of Raman scattering

The penetration depth of the Raman measurements was studied measuring a layered structure consisting of a 2 mm thick layer of amorphous xylitol or amorphous xylitol-silica dispersion, 1 mm of ibuprofen and a thick layer of γ-indomethacin (Fig. 3a). All layers were separated using Mylar film. Spectra were collected at 0, 3 and 6 h from sample preparation to ensure complete recrystallization of the amorphous xylitol.

To study the extent of over-representation of the sample surface, a sample containing 1 mm of crystalline xylitol and 1 mm of ibuprofen (Fig. 3b) was studied. Raman spectra were collected from both sides of the bilayer system in triplicate.

2.2.4. Wide-angle X-ray scattering (WAXS)

A Rigaku rotating-anode based X-ray set-up built at the University of Helsinki (Kontro et al., 2014) was used for the WAXS measurements. The samples were measured with perpendicular transmission geometry in ambient temperature using Cu $K\alpha_1$ wavelength (0.1541 nm). The beam size for the WAXS measurements was 1 mm^2 because a larger beam size would cause significant broadening of the diffraction peaks. In order to obtain a good temporal resolution, a Pilatus 1 M detector was used and exposures of 5 or 15 s were measured continuously over the experiment (15 min for the crystalline xylitol reference, 90 min for amorphous xylitol and 150 min for the amorphous xylitol combined with 10-weigth percent silica). These exposures were averaged over a time period of 60 s to improve signal-to-noise ratio. Each averaged exposure was corrected as described in Dixon et al. (2015). The ambient relative humidity was between 19.2 and 31.3% and the ambient temperature was between 28.7 and 29.3 °C during the measurements.

An amorphous xylitol scattering pattern was obtained from the average of the first three minutes of the amorphous xylitol measurement. A crystalline xylitol model was obtained by reading in peak positions and relative heights from the crystalline xylitol measurement. A scattering pattern obtained from a separate measurement of pure silica and the amorphous xylitol scattering pattern were used to assess the contribution of silica in the xylitol-silica sample. Least-squares fitting was used to assess the relative scattering contribution of the mesoporous silica (13%). The relative amount of silica was assumed constant and this contribution was subtracted from all the data points of the xylitol-silica measurements. After the subtraction, the corrected scattering data represents only the xylitol component.

The crystallinity value was obtained using least-squares-fitting of a linear superposition of the sharp diffraction peaks (modeled as Gaussian) and the amorphous xylitol scattering pattern. To account for small changes in sample position, crystallite sizes and crystalline structure, peak positions were allowed to vary 0.5° in position, 30% in relative height and 50% in peak width. The xylitol

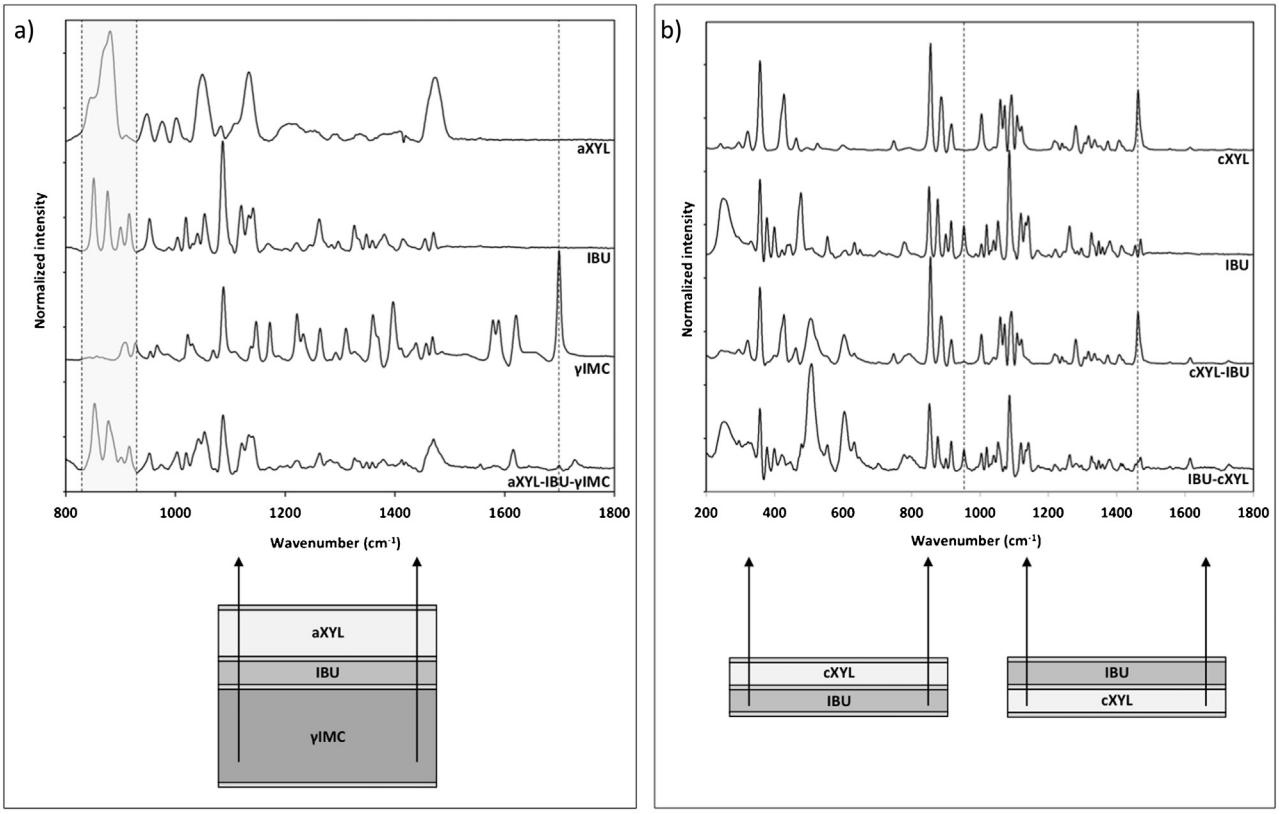

Fig. 3. Depth of detection of the Raman-spectrometer used in the present study. (a) Raman spectra of amorphous xylitol (aXYL), ibuprofen (IBU), γ-indomethacin (γIMC) and the spectrum measured of a layered system consisting of 2 mm of aXYL and 1 mm of IBU on a thick layer of γIMC (aXYL-IBU- γIMC); (b) Raman spectra of crystalline xylitol (cXYL), ibuprofen (IBU) and a layered system consisting of 1 mm of cXYL and IBU measured with cXYL or IBU above (cXYL-IBU and IBU-cXYL, respectively).

crystallinity value was then calculated from the areas under the sample intensity curve $I_{xylitol}$ and the amorphous contribution I_{am} as

$$C = 1 - \frac{\int_0^{\infty} I_{am}\,dq}{\int_0^{\infty} I_{xylitol}\,dq} \approx 1 - \frac{\int_{10^\circ}^{50^\circ} I_{am}\,d2\theta}{\int_{10^\circ}^{50^\circ} I_{xylitol}\,d2\theta} \quad (1)$$

The xylitol crystallinity values were normalized with the average crystallinity value of the crystalline xylitol measurement.

2.2.5. Differential scanning calorimetry

The solid state of the raw materials, freshly prepared samples and end products were tested using differential scanning calorimetry (DSC; DSC823e, Mettler-Toledo Inc., Switzerland). The samples were cooled to −50 °C and then heated to 0 °C. After that, the samples were re-cooled to −50 °C and heated up to 140 °C. The heating was performed with a heating rate of 10 °C/min. The amounts of freshly prepared samples were 10.55 mg for the amorphous sample, 5.05 mg for the amorphous xylitol-silica sample and 7.90 mg for the crystalline sample. The samples measured 6 h after preparation had masses of 5.63 and 5.62 mg for xylitol and xylitol-silica dispersion, respectively.

3. Results and discussion

3.1. Raman spectrometry

The Raman-spectrum of amorphous xylitol differed from that of crystalline xylitol in ways typical to an amorphous spectrum (Fig. 4), *i.e.* peak broadening and loss of detail in the spectral structure (*e.g.* Chieng et al., 2011; Ward et al., 2005). In their study on amorphous sorbitol, Ward et al. (2005) used the full-width at half-maximum of the peak caused by CCO-stretching to distinguish between amorphous and crystalline sorbitol, but they did not, however, quantify the amount of crystalline and amorphous sorbitol. The similarity in peak positions and overlapping features did not permit assessing crystallinity using peak intensities, areas or full-width at half maximum in the present study, but the spectral features were distinct enough to allow quantification using PLS-modeling, as described by Johansson et al. (2005). As peaks merged in the spectrum of amorphous xylitol and there were overlapping peaks in the spectra of crystalline and amorphous xylitol, using a wider wavenumber range in modeling was justified (Savolainen et al., 2007).

When monitoring the crystallization of amorphous xylitol using Raman (Fig. 5), the spectrum of the initial state of the sample corresponds to that of amorphous xylitol. The peak intensity of the spectrum decreased until no distinct spectral features were noticed at 5 min at T = 21 °C, after which the characteristic spectral features of crystalline xylitol gradually emerge in the spectra as the xylitol crystallizes. Visual inspection of the system showed that the amorphous form was opalescent after sample preparation. The opalescence gradually reduced and the sample became clear, until the opalescence gradually reoccurred as the crystallization progressed. The intermediate region lacking distinct spectral features between having amorphous substance and recrystallization could be due to formation of a rubbery state, seen as increased clarity of the sample, as the measurement was done in temperatures clearly above the glass transition temperature of xylitol.

When studying the penetration depth of Raman, features of the spectral pattern of ibuprofen (peaks at 850, 875, 898 and 914 cm^{-1}) were detected through 2 mm of amorphous xylitol and features of γ-indomethacin (peak at 1689 cm^{-1}) were detected through a 3 mm thick sample consisting xylitol and ibuprofen (Fig. 3a). This indicates that the Raman spectrometer used in the present study was able to detect changes from all depths of the 2 mm thick xylitol samples. The intensity of the peak at 1689 cm^{-1} in the Raman spectrum of γ-indomethacin did not depend on whether it was detected through the fully amorphous or the crystalline xylitol, indicating that the penetration depth was unaffected by the solid state of xylitol. The inclusion of 10% (m/m) of silica dispersed in the xylitol did not affect the outcome of the penetration depth studies. When studying the xylitol-ibuprofen bilayer system, the uppermost sample was clearly overrepresented, indicating that even though the whole sample is represented in the Raman spectra in

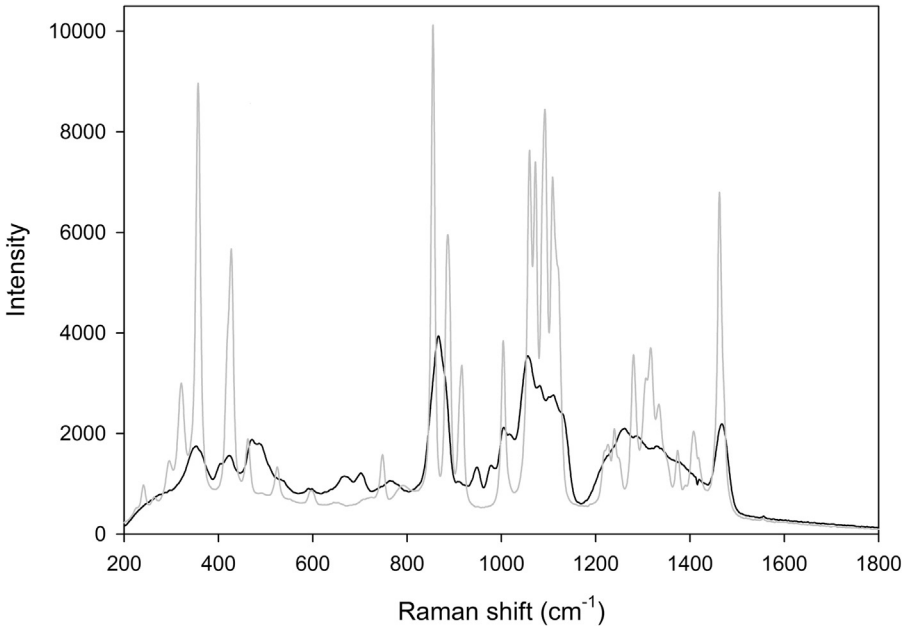

Fig. 4. Typical Raman spectra of amorphous (black) and crystalline xylitol (gray).

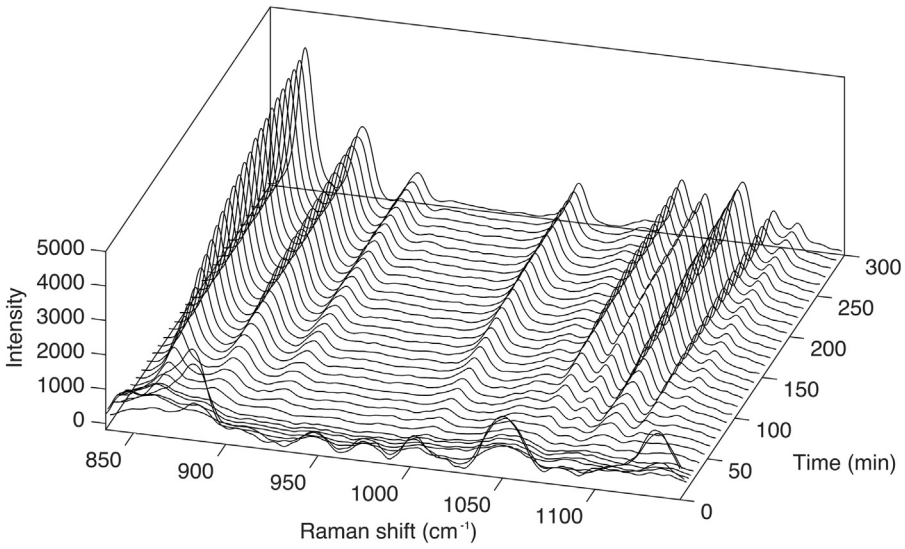

Fig. 5. Crystallization of amorphous xylitol measured with Raman spectroscopy at T = 21 °C. The spectra shown are taken with 4-min intervals from 0 to 20 min and in 10-min intervals from 20 to 300 min.

the present study, the Raman measurements are surface-sensitive (Fig. 3b).

3.2. Multivariate modeling

PLS-models were built using the Raman spectra of reference samples with known degrees of crystallinity. The best model was achieved from 2nd derivatives of MSC-corrected spectra, although 2nd derivatives of SNV-corrected spectra produced an almost equally good model. The models had three components and R^2 and Q^2-values of 0.972 and 0.970 and 0.971 and 0.969 respectively. It is known that Raman-spectra are affected by variations in particle size, sample packing, fluorescence, instrument reproducibility and intra- and interday variatons in intensity (Heinz et al., 2007; Pellow-Jarman et al., 1996). The Raman-spectra in the present study had fluctuations in intensity and baseline variation, which explains the suitability of the commonly used MSC, SNV and 2nd derivatization as pretreatment methods (Johansson et al., 2005; Strachan et al., 2007; Rinnan et al., 2009). 2nd derivatives remove both baseline shifts and linear trends, whereas MSC is capable of removing both additive and multiplicative errors of spectra (Rinnan et al., 2009). MSC requires an external reference spectrum, most often the average of the calibration set. Since MSC and SNV often produce very similar outcomes as in this case (Rinnan et al., 2009), and SNV uses the average of the sample spectrum for normalization, the model built from 2nd derivatives of SNV-treated spectra could be used in real-time monitoring of crystallization as described by Savolainen et al. (2007).

The effect of the mesoporous silica on the Raman-spectrum of xylitol was examined. In the Raman spectrum of Syloid 244FP there were no distinct peaks, but areas with broad increases in intensity similar to local baseline shifts. In the wavenumber area used for

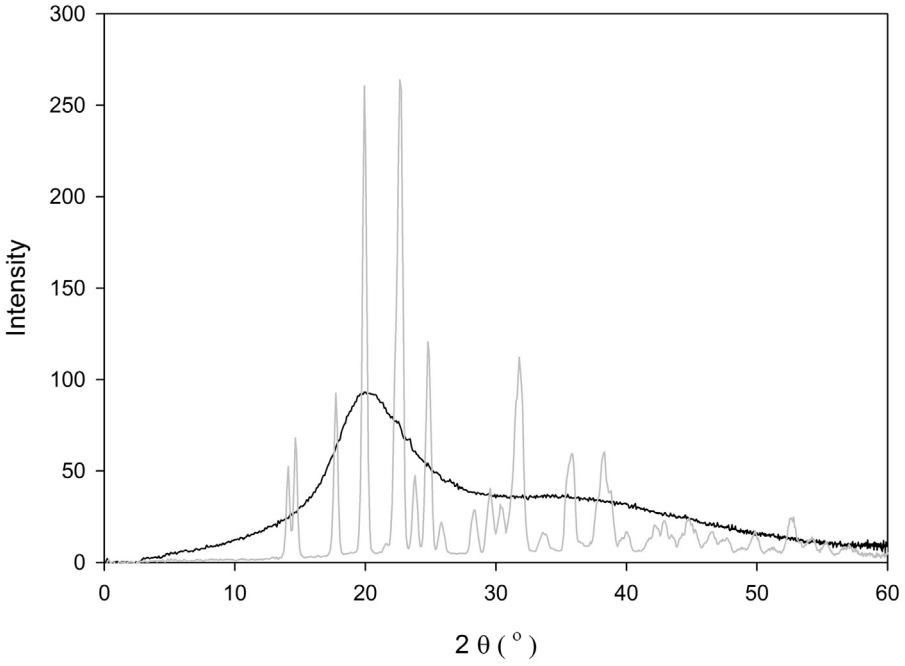

Fig. 6. Typical WAXS intensity curves of amorphous xylitol (black) and crystalline xylitol (gray).

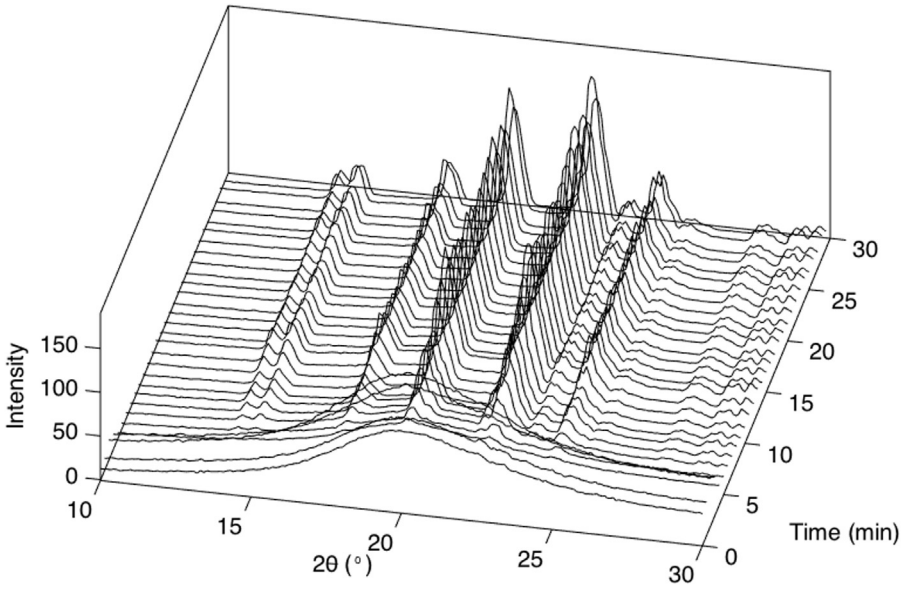

Fig. 7. Crystallization of amorphous xylitol measured with WAXS. Diffraction patterns shown were taken in 1-min intervals for 30 min.

analysis in the present study the effect of Syloid 244FP on the spectrum was similar to that of a slightly elevated baseline.

3.3. Wide angle X-ray scattering (WAXS)

In the diffractograms from WAXS the crystalline sample showed a typical diffraction pattern of orthorhombic xylitol when compared with data from the Cambridge Crystallographic Data Centre (CCDC), whereas the amorphous counterpart showed a characteristic amorphous halo (Fig. 6).

When studying the crystallization of amorphous xylitol using WAXS the first crystalline peaks emerged after five minutes, followed by a rapidly increasing relative contribution of crystalline peaks of the orthorhombic form of xylitol (Fig. 7). The positions of the peaks did not change during the experiment, indicating that the unit cell dimensions of crystalline xylitol did not change.

3.4. Recrystallization of xylitol and xylitol-silica solid dispersions

The recrystallization rate of amorphous xylitol-silica dispersions was higher than the recrystallization rate of amorphous xylitol measured with Raman-spectrometry (Fig. 8). The replicate measurements were performed in slightly different temperatures, which might explain observed between measurements, since crystallization is known to be temperature dependent (Bhugra and Pikal, 2008). In the present study, increasing the temperature caused the rate of crystallization to increase as measured with Raman. Increasing the temperature increases molecular motion and reduces viscosity, which both favor crystallization (Bhugra and Pikal, 2008; Yu, 2016). When the temperature was increased from T = 21 °C to T = 29 °C, the difference in rate of crystallization between pure xylitol and xylitol-silica dispersion became less significant. This can be explained by the higher temperature and lower viscosity of the super-cooled liquid having a more pronounced impact on bulk crystallization than on surface crystallization.

The recrystallization of xylitol was faster in T = 29 °C compared to ambient conditions of T = 21 °C (Figs. 8 and 9). This can be attributed to the temperature dependence of crystal growth (Bhugra and Pikal, 2008), since the ambient temperature during Raman measurements in ambient conditions was clearly lower than during the WAXS-experiments and Raman experiments in

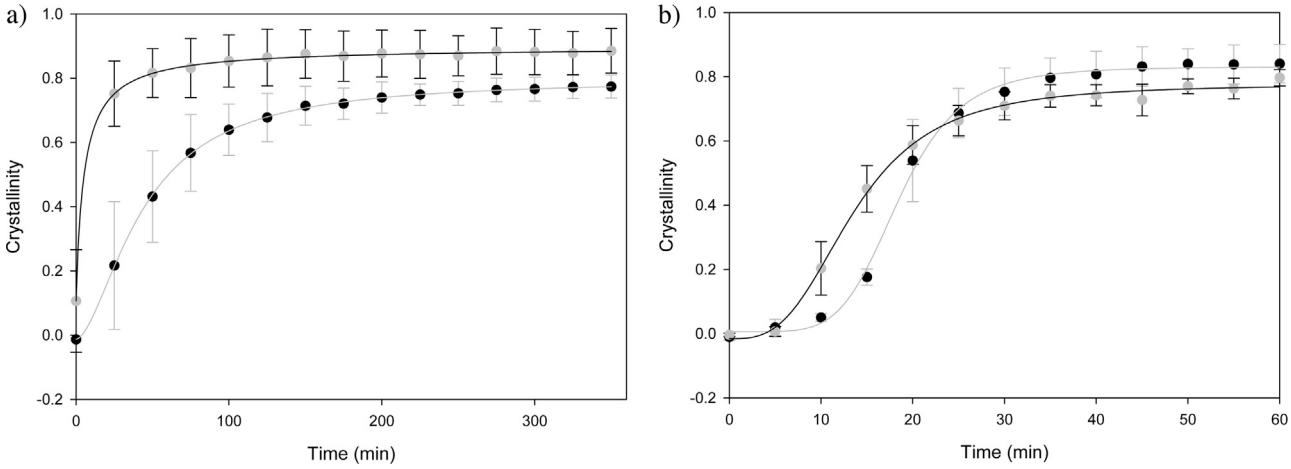

Fig. 8. Averaged crystallization curves of the Raman measurements for amorphous xylitol sample (black dots and gray line) and amorphous xylitol-silica dispersion (gray dots and black line). (a) ambient conditions (T = 20.1–21.6 °C and RH% = 21–36) (b) elevated temperature (T = 28.5–29.5 °C and RH% = 19–25%).

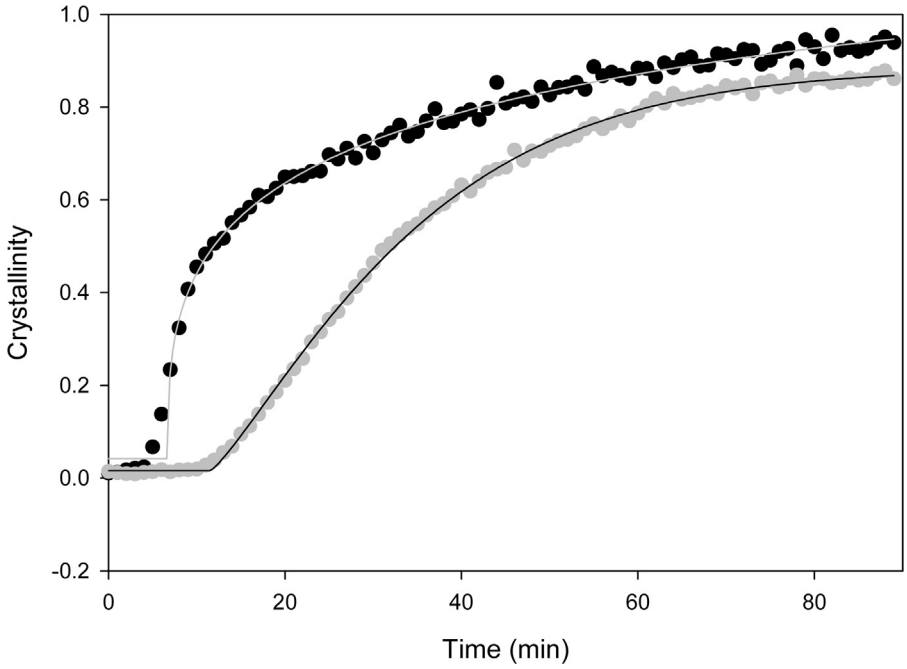

Fig. 9. Crystallization of amorphous xylitol sample (black) and amorphous xylitol–silica mixture (grey) measured with WAXS.

elevated temperature. Based on the WAXS results, the rate of crystallization was slower for the solid dispersion, opposite to the Raman measurements (Fig. 9). When recrystallization of xylitol in T = 29 °C was measured using Raman, the recrystallization rate of pure xylitol was comparable to that measured using WAXS (Figs. 8b and 9). The rate of crystallization was higher for xylitol-silica dispersions measured with Raman as compared to WAXS. Bulk diffusion is promoted over surface diffusion at temperatures above T_g while surface diffusion becomes instable due to viscous flow on the surface (Yu, 2016). Still, even at elevated temperatures, Raman measurements showed differences compared to WAXS that could be attributed to surface crystallization, since the measurement geometry of the Raman measurements favors detection of surface events.

The different effects of the mesoporous silica on the crystallization rate of xylitol observed with Raman spectrometry and WAXS can be explained by three different factors with an additive effect on the measurement outcome. Firstly, the difference in measurement setup between Raman and WAXS is expected to affect the result, as the Raman measurements were done with a backscattering geometry while the WAXS measurements were done with perpendicular transmission geometry. The results from Raman spectroscopy thus more pronouncedly show crystallization events at or near the surface of the sample, as described by Priemel et al. (2012). The findings regarding penetration depth in the present study also confirm that the surface was overrepresented in the results obtained using Raman compared to those from WAXS-measurements (Fig. 3a and b).

Secondly, Priemel et al. (2012) showed that nanocrystalline indomethacin was detected as crystalline when using Fourier transform attenuated total reflectance spectroscopy (FT-ATR-IR) but amorphous when using X-ray powder diffractometry (XRPD). Vibrational spectroscopy, such as IR- or Raman spectroscopy, shows both intra- and intermolecular vibrations and therefore detects very short-range disorder, whereas WAXS detects lack of order on a crystallite or particle level. Thus, WAXS cannot definitively distinguish whether the sample is amorphous or nano-crystalline, but with insufficient long-range order (Bates et al., 2006). Ueda et al. (2014) found that the rate of crystallization of amorphous indomethacin was faster when measured using Raman compared with XRPD. They found that Raman has a lower level of detection than XRPD, possibly due to nano-crystalline material and crystal nuclei appearing amorphous using XRPD but are detectable using Raman, as also described by Savolainen et al. (2009). Also Tian et al. (2007) reported underestimation of the level of crystallinity of amorphous carbamazepine compacts using XRPD compared to Raman spectroscopy. They attributed the variation in crystallinity between methods to differences in diffraction patterns of the calibration samples used in the models to describe degree of crystallinity and the crystallized drug on the compact surfaces, caused by decreased crystal size and differences in crystal morphology and preferential orientation.

Thirdly, the difference might arise from differences in crystallization rate on the surface and in the bulk of the samples. Tian et al. (2007) analyzed the surface of carbamazepine compacts and ground compacts. The results show higher degrees of crystallinity on the surface of the compacts that in ground compacts both using Raman and XRPD, indicating that the higher crystallinity detected using Raman could be due to the crystallization itself being more pronounced on the compact surface. Crystallization on the surface of amorphous particles has been reported to be considerably faster than in the bulk using griseofluvin, indomethacin and nifedipine (Zhu et al., 2010, 2008; Wu et al., 2007; Wu and Yu, 2006) due to surface molecules having a higher mobility than molecules in the bulk. Zhu et al. (2010, 2008) and Wu et al. (2007) showed that surface crystallization could be suppressed by coating the sample surface. Nanubolu and Burley (2012) and Wu et al. (2007) reported that the crystallization kinetics of amorphous drugs changed when covering the sample using a coverslip and thus restricting the surface molecule mobility. In the present study the surface of the sample was covered with Mylar-film, but the coverage might not have been close enough to restrict the mobility of the surface molecules. One additional possible explanation for the pronounced

surface crystallization of quench-cooled samples is heat transmission, since the surface of the sample presumably reaches room temperature earlier than the bulk.

Watanabe et al. (2001) suspended silicon dioxide in molten indomethacin and quench-cooled the mix to obtain an amorphous sample. They found that silicon dioxide decreased the rate of recrystallization of indomethacin due to interactions between hydroxyl groups on the surface of the silicon dioxide particles and the polar groups of indomethacin. Takeuchi et al. (2005) also reported increased stability of solid dispersions containing amorphous indomethacin and silica particles. Mártha et al. (2014) studied co-grinding of clopidogrel and silicon dioxide, and found that hydrogen bonding between silanol groups on the surface of silicon dioxide particles and the drug molecule resulted in a more stable amorphous structure. Hydrogen bonding similar to that between hydroxyl groups on the carrier surface and drug molecules could explain the decrease in crystallization rate in the bulk of the xylitol-silica dispersion in the present study, considering the molecular structure of xylitol (Watanabe et al., 2001; Takeuchi et al., 2005; Xu et al., 2013; Mártha et al., 2014).

One must also consider that when a foreign surface is added to an amorphous system, heterogeneous nucleation is favored. Hellrup and Mahlin (2011) investigated the stabilizing effect of micro-sized filler particles dispersed in freeze-dried sucrose. They found that the filler particles increased the glass transition temperature, and concluded that the filler particles decrease the molecular mobility and hence stabilized the amorphous structure. They also discovered small amounts of crystallinity in the sucrose samples, but these did not alter the stability of the amorphous state. Consequently they could not confirm any stabilizing effects due to increased heterogenous nucleation. Bhatt et al. (2015) showed that in spray dried solid dispersions containing crystalline mannitol and amorphous celecoxib, the mannitol acted as a surface for heterogenous nucleation while at the same time being a physical barrier preventing crystal growth, leading to a nanocrystalline solid dispersion. The silica added to the xylitol in the present study was expected to increase heterogenous nucleation, rendering more pronounced nucleation and crystal growth in the bulk of the sample, which could promote the formation of similar structures as described by Hellrup and Mahlin (2011) and Bhatt et al. (2015).

The surface crystallization studies by Zhu et al. (2010, 2008), Wu et al. (2007), and Wu and Yu (2006) were completed with amorphous substances below the glass transition temperature (T_g), while the present study was performed above T_g. In the present study, solid xylitol was molten and rapidly re-solidified in liquid nitrogen at a temperature approximately 170 K below Tg. When a melt is rapidly cooled to temperatures significantly below Tg, the molecular motion rapidly decreases and the system reaches a non-equilibrium state (Yu, 2016). Below Tg, recrystallization of the amorphous solid is emphasized on the particle surfaces. This is due to the fact that molecules on the surface have more degrees of freedom in their movement. This results in pronounced surface diffusion of molecules causing crystal growth to occur laterally along the surface and away from the surface. When the temperature of the sample is increased to T_g and above, the sample becomes rubbery, and the viscosity decreases with growing temperature. This results in viscous flow, which overrides the effects of surface diffusion and, according to Yu (2016), leads to lower and instable rates of surface crystallization. When the viscosity of a super-cooled liquid decreases, the rate of crystallization increases as the diffusion of molecules in the bulk is facilitated.

For crystal growth to occur effectively on the surface of an amorphous glass, the surface needs to be rigid (Yu, 2016). Above T_g, amorphous substances experience liquid-like flow to some extent, which might slow down the surface crystal growth and render it instable. When silica is added to the system, the amount of free surfaces increase and there is interaction between the silica particles and xylitol-molecules, the viscosity of the melt increases and as a result of the structural rigidification that follows, the prerequisites for surface crystallization might be promoted.

As reported by *e.g.* Riikonen et al. (2009) and Mellaerts et al. (2008), substances loaded into the pores of porous carriers remain amorphous if the pore is small enough to prevent the nuclei from reaching the critical size for crystallization. Furthermore, even if the pore size allows crystallization, the substance in close vicinity to the pore walls remains amorphous. Mellaerts et al. (2008) described how molten ibuprofen and itraconazole enter pores, and found that the drug loading is impaired if the melt has a high viscosity. In the present study, the xylitol melt seemed fairly viscous, which could result in only small amounts of xylitol entering the silicon dioxide pores. The lower level of crystallinity in the xylitol-silica dispersions observed in Figs. 9 and 8b could be explained by a small amount of xylitol being absorbed in the pores of the silica and consequently remaining amorphous, while the remaining xylitol outside the pores crystallizes.

Hellrup et al. (2015) studied the effect of a nanofiller (fumed silica) on the recrystallization of spray-dried amorphous lactose. They found that crystallization of amorphous systems is inhibited through confinement, *i.e.* entrapment within pores, compartmentalization, *i.e.* isolating amorphous compartments from each other and rigidification, *i.e.* molecular interactions between amorphous molecules and solid surfaces. In the present study, xylitol melt is mixed with non-ordered mesoporous silica. The results showed signs of confinement as described by *e.g.* Mellaerts et al. (2008) and rigidification as described by *e.g.* Watanabe et al. (2001), which in combination could explain the lower crystallization rate and lower level of end crystallinity observed using WAXS. Although the volume fraction of silica in the system was rather high due to its low density, no conclusive evidence indicating compartmentalization of amorphous xylitol due to silicon dioxide particles as described by Hellrup et al. (2015), Priemel et al. (2013) and Hellrup and Mahlin (2011) could be found. Still, compartmentalization leading to nanocrystalline structures having a resemblance to those described by Priemel et al. (2012) and Bhatt et al. (2015) cannot be conclusively ruled out solely based on Raman and WAXS measurements.

Samples from xylitol and xylitol-silica dispersions were visually inspected using a microscope following Raman-measurements (Fig. 10a and c). The crystal size of xylitol-silica dispersions (Fig. 10c) was clearly smaller than that of pure xylitol (Fig. 10a) based on visual inspection. No conclusive evidence of varying crystal size on the surface compared to the bulk could be observed. Interestingly, when melting the xylitol sample mentioned onto an object glass and quench-cooling the system in liquid nitrogen, no signs of re-crystallization of parts of the sample could be observed within days of sample preparation (Fig. 10b), and when crystallization occurred, the crystallite size was significantly larger than in the ground samples (Fig. 10a). A possible reason explaining the difference in crystallization behavior is process-induced nucleation in the ground sample. One could assume that this process-induced nucleation would be highly surface-oriented simply due to the nature of particle size reduction. The xylitol-silica dispersions showed no delay in onset of crystallization when melting the sample on an object glass and quench-cooling it in liquid nitrogen. This further supports the hypothesis of process-induced surface nucleation of ground xylitol samples and pronounced heterogeneous nucleation of xylitol-silica dispersions. The particle size of the non-ground recrystallized xylitol-silica dispersion was similar to the ground xylitol-silica dispersions on visual inspection. This can be seen as evidence supporting the hypothesis of silica suppressing crystals growing in size while still favoring

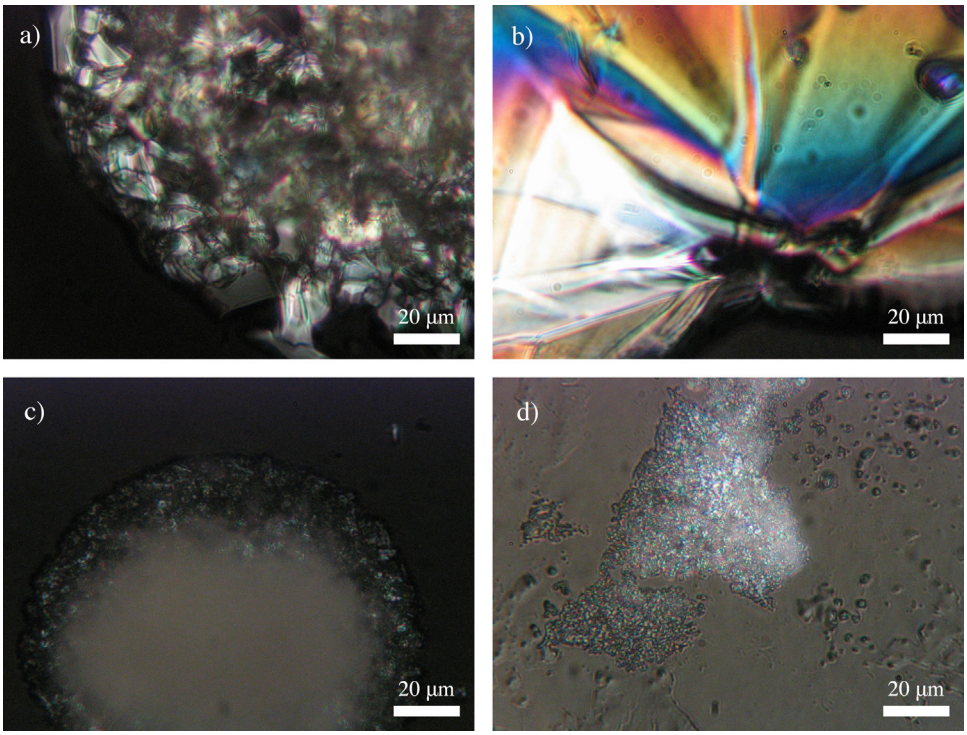

Fig. 10. Microscope images ground (a and c) and non-ground (b and d) xylitol (a and b) and xylitol-silica dispersion (c and d).

heterogenous nucleation, similar to that reported by Priemel et al. (2012) and Bhatt et al. (2015).

The crystallization kinetics of the samples measured using WAXS and one representative sample containing only xylitol and one representative sample containing xylitol-silica dispersion measured using Raman at T = 21 °C as a function of time was investigated using the Avrami-equation $y = 1 - e^{(-k(t-\tau)^n)}$, in which y is the amount of crystalline substance, k describes the rate of conversion, t is time, τ is the lag time before onset of crystallization and n describes the dimensionality of crystal growth (Tripathi et al., 2015; Çelikbilek et al., 2012). As the crystallization curves showed signs of a two-phased growth mechanism, only the initial phase of rapid growth was investigated. If grinding was assumed to cause site saturated nucleation, values of $n = 1$ would imply one-dimensional growth, $n = 2$ two-dimensional growth and $n = 3$ three-dimensional growth. The Avrami constant n was found to be approximately 2.0 in Raman measurements and approximately 2.8 WAXS measurements regardless of sample type. This can be seen as further evidence supporting that Raman measures surface crystallization, whereas WAXS measurements describe the overall crystallinity.

In the present study WAXS and Raman at T = 21 °C and T = 29 °C showed different end state crystallinity. The variation in level of crystalline content in late stages of crystallization can be explained through the effect of particle size on the crystallization rate when surface crystallization is dominant over bulk crystallization. As described in a recent review by Yu (2016), when the particle surfaces are fully crystalline, the crystalline content plateaus and the overall crystallization rate is dominated by significantly slower bulk crystallization. The level of the plateau is lower with increasing particle size.

In Fig. 9, the overall rate of crystallization, as measured with WAXS, seemed to clearly decrease for a prolonged period of time towards the end of crystallization with pure xylitol as compared to the xylitol-silica dispersion. This kinetic behavior is in line with the description in Yu (2016) of a biphasic crystallization rate caused by surface crystallization preceding bulk crystallization. Signs of similar behavior can be seen in Raman measurements, but not as clearly as with WAXS. Consequently, considering the difference in measurement geometry, surface crystallization seems to be dominant over bulk crystallization.

3.5. Thermal analysis

In the DSC-thermograms (Fig. 11), amorphous xylitol and amorphous xylitol-silica dispersions both showed glass transition. In the thermogram of amorphous xylitol, a wide exothermic recrystallization peak was detected after the glass transition, followed by a clear endothermic melting peak corresponding to the melting point of xylitol (92–96 °C). No differences in glass transition were detected between the first and second cooling of the sample. The onset glass transition temperature (T_g) for amorphous xylitol was −23.3 °C, which corresponds well with the value of −24.1 °C for waterless xylitol reported by Talja and Roos (2001). The slight difference could be explained with the heating rate, which was 10 °C/min in the present study and 5 °C/min in Talja and Roos (2001).

The T_g of xylitol-silica dispersions was −32.4 °C, which is clearly lower than that of waterless xylitol. Mellaerts et al. (2008) reported a decrease in T_g of itraconazole loaded in mesoporous silica particles, and attributed the decrease to confinement of itraconazole in the pores of the carrier material and to the increased surface-to-volume ratio of the adsorbed itraconazole phase. The decrease of the glass transition temperature in the present study could partially be attributed to confinement of xylitol in the pores of Syloid 244 FP. No melting peak was detected for the xylitol-silica dispersion in the present study. Similar behavior was reported by Kinnari et al. (2011). They studied itraconazole loaded Syloid 244FP, and explained the lack of melting peak to itraconazole being amorphous. Mellaerts et al. (2008) found similar results, including an absence of the crystallization peak as in the present study. Since there was a broad exothermic peak in the DSC-thermogram

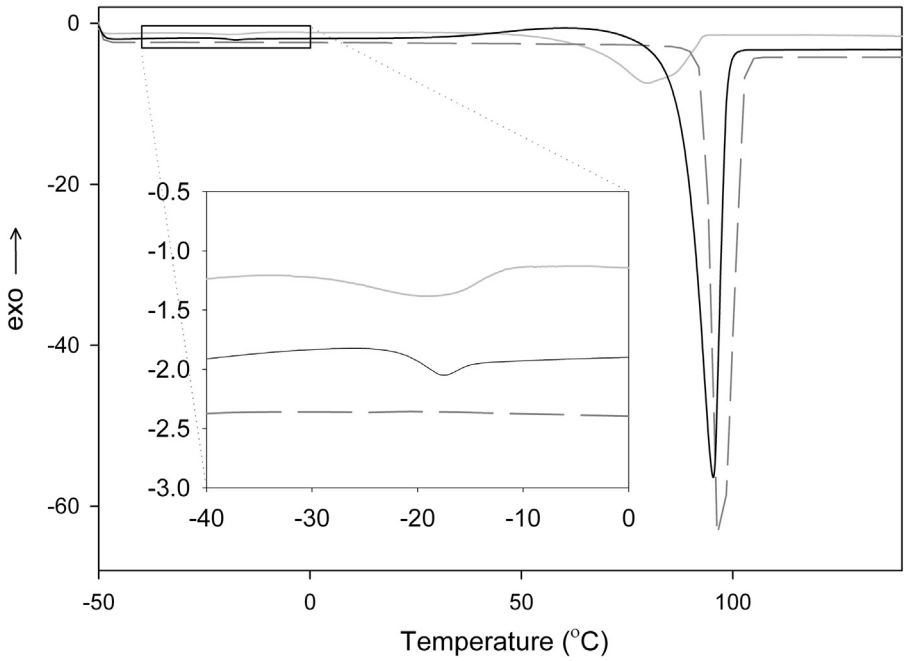

Fig. 11. Typical DSC thermograms of amorphous xylitol (black), mixture of amorphous xylitol and silica (light grey) and crystalline xylitol (dark grey, dashed).

starting around 40 °C that corresponds well with that reported for evaporation of water (*e.g.* Artiaga et al., 2005), and as Talja and Roos (2001) found that water content has a significant effect on the T_g of xylitol, with a value of – 53 °C reported for xylitol samples containing 10% of water, the presence of water in the xylitol-silica dispersions in the samples analyzed using DSC cannot be exluded.

Hellrup and Mahlin (2011) discovered that micro-sized filler particles stabilized freeze-dried amorphous sucrose. They found that there is a critical relative humidity threshold, above which the stabilizing effect of the filler micro-particles was lost. The results in the present study indicate that the xylitol-silica dispersions studied with DSC contained some atmospheric water that most likely condensed on the sample surface immediately after evaporation of the liquid nitrogen, which was reflected in the T_g. Although measures were taken to avoid water exposure during the Raman and WAXS-measurements, complete absence of water cannot be confirmed. In addition to plasticizing the amorphous sample and thus increasing molecular mobility (*e.g.* Andronis et al., 1997), the water might inhibit the stabilizing effect of the silicon dioxide particles as described by Hellrup and Mahlin (2011). After a recrystallization time of 6 h, none of the samples in the present study showed any signs of glass transition in the DSC-thermograms, indicating that all samples were fully crystalline at the end of Raman measurements.

4. Conclusions

Quench-cooled and cryo-ground amorphous xylitol recrystallized rapidly in room temperature showing features of surface crystallization, and could be used as a model system for rapid recrystallization from the amorphous state. Introducing 10% (m/m) of non-ordered mesoporous silica to the system decreased the overall rate of crystallization in the sample, as detected by WAXS. Furthermore, adding silica to the system seemed to facilitate heterogeneous nucleation and decreased the crystal size of xylitol.

Raman spectroscopy can be used when studying the recrystallization of amorphous xylitol. The amorphous form of xylitol and crystalline content can be detected rapidly in seconds and accurately even in trace amounts, which enables real-time monitoring of crystallization. The Raman instrument in the present study was capable of measuring on a depth more than 3 millimeters. Still, the surface is clearly overrepresented in the signal, which enables monitoring surface crystallization of xylitol.

The transmission WAXS-setup used in the present study enables making conclusions on the total crystallization rate of the amorphous sample, consisting of both surface crystallization and bulk crystallization, and is thus a valuable complement to the surface-dominated Raman measurements. In addition, the WAXS-setup allows relatively short integration times, which enables accurate real-time monitoring of crystallization. Raman spectroscopy and transmission WAXS provide valuable complementary information in real-time monitoring of rapidly crystallizing amorphous systems.

Acknowledgements

The work has been supported by Academy of Finland (Suomen Akatemia).

References

Andronis, V., Yoshioka, M., Zografi, G., 1997. Effects of sorbed water on the crystallization of imdomethacin from the amorphous state. J. Pharm. Sci. 86 (3), 346–351.
Artiaga, R., Naya, S., Garcìa, A., Barbadillo, F., Garcìa, L., 2005. Subtracting the water effect from DSC curves by using simultaneous TGA data. Thermochim. Acta 428, 137–139.
Bates, S., Zografi, G., Engers, D., Morris, K., Crowley, K., Newman, A., 2006. Analysis of amorphous and nanocrystalline solids from their X-ray diffraction patterns. Pharm. Res. 23 (10), 2333–2349.
Bhatt, V., Shete, G., Bansal, A.K., 2015. Mechanism of generation of drug nanocrystals in celecoxib: mannitol nanocrystalline solid dispersion. Int. J. Pharm. 495 (1), 132–139.
Bhugra, C., Pikal, M.J., 2008. Role of thermodynamic, molecular and kinetic factors in crystallization from the amorphous state. J. Pharm. Sci. 97 (4), 1329–1349.
Carson, J.F., Waisbrot, S.W., Jones, F.T., 1943. New form of crystalline xylitol. J. Am. Chem. Soc. 65 (9), 1777–1778.
Çelikbilek, M., Ersundu, A.E., Aydın, S., 2012. Crystallization kinetics of amorphous materials. In: Yitzhak Mastai (Ed.), Advances in Crystallization Processes, , pp. 127–162.

Chieng, N., Rades, T., Aaltonen, J., 2011. An overview of recent studies on the analysis of pharmaceutical polymorphs. J. Pharm. Biomed. Anal. 55 (4), 618–644.
de Veij, M., Vandenabeele, P., De Beer, T., Remon, J.P., Moens, L., 2009. Reference database of Raman spectra of pharmaceutical excipients. J. Raman Spectrosc. 40, 297–307.
Diogo, H.P., Pinto, S.S., Moura Ramos, J.J., 2007. Slow molecular mobility in the crystalline and amorphous solid states of pentitols: a study by thermally stimulated depolarisation currents and by differential scanning calorimetry. Carbohydr. Res. 342, 961–969.
Dixon, P.G., Ahvenainen, P., Aijazi, A.N., Chen, S.H., Lin, S., Augusciak, P.K., Borrega, M., Svedström, K., Gibson, L.J., 2015. Comparison of the structure and flexural properties of Moso: guadua and Tre Gai bamboo. Constr. Build. Mater. 90, 11–17.
Dong, Y.-D., Boyd, B.J., 2011. Applications of X-ray scattering in pharmaceutical science. Int. J. Pharm. 417, 101–111.
Dunitz, J.D., Bernstein, J., 1995. Disappearing polymorphs. Acc. Chem. Res. 28, 193–200.
Hancock, B.C., Zografi, G., 1997. Characteristics and significance of the amorphous state in pharmaceutical systems. J. Pharm. Sci. 86 (1), 1–12.
Hasegawa, S., Ke, P., Buckton, G., 2009. Determination of the structural relaxation at the surface of amorphous solid dispersion using inverse gas chromatography. J. Pharm. Sci. 98 (6), 2133–2139.
Heinz, A., Savolainen, M., Rades, T., Strachan, C.J., 2007. Quantifying ternary mixtures of different solid-state forms of indomethacin by Raman and near-infrared spectroscopy. Eur. J. Pharm. Sci. 32 (3), 182–192.
Hellrup, J., Mahlin, D., 2011. Pharmaceutical micro-particles give amorphous sucrose higher physical stability. Int. J. Pharm. 409 (1–2), 96–103.
Hellrup, J., Alderborn, G., Mahlin, D., 2015. Inhibition of recrystallization of amorphous lactose in nanocomposites formed by spray-drying. J. Pharm. Sci. 104 (11), 3760–3769.
Johansson, J., Pettersson, S., Folestad, S., 2005. Characterization of different laser irradiation methods for quantitative Raman tablet assessment. J. Pharm. Biomed. 39, 510–516.
Kinnari, P., Mäkilä, E., Heikkilä, T., Salonen, J., Hirvonen, J., Santos, H.A., 2011. Comparison of mesoporous silicon and non-ordered mesoporous silica materials as drug carriers for itraconazole. Int. J. Pharm. 414 (1–2), 148–156.
Kontro, I., Wiedmer, S.K., Hynönen, U., Penttilä, P.A., Palva, A., Serimaa, R., 2014. The structure of *Lactobacillus brevis* surface layer reassembled on liposomes differs from native structure as revealed by SAXS. Biochim. Biophys. Acta 1838 (8), 2099–2104.
Laitinen, R., Löbmann, K., Strachan, C.J., Grohganz, H., Rades, T., 2013. Emerging trends in the stabilization of amorphous drugs. Int. J. Pharm. 453, 65–79.
Limnell, T., Santos, H.A., Mäkilä, E., Heikkilä, T., Salonen, J., Murzin, D.Y., Kumar, N., Laaksonen, T., Peltonen, L., Hirvonen, J., 2011. Drug delivery formulations of ordered and nonordered mesoporous silica: comparison of three drug loading methods. J. Pharm. Sci. 100 (8), 3294–3306.
Mártha, C., Jójárt-Laczkovich, O., Szabó-Révész, P., 2014. Effect of co-grinding on crystallinity of clopidogrel bisulfate. Chem. Eng. Technol. 37 (8), 1393–1398.
Matousek, P., Clark, I.P., Draper, E.R.C., Morris, M.D., Goodship, A.E., Everall, N., Towrie, M., Finney, W.F., Parker, A.W., 2005. Subsurface probing in diffusely scattering media using spatially offset Raman spectroscopy. Appl. Spectrosc. 59 (4), 393–400.
Mellaerts, R., Jammaer, J.A.G., Van Soeybroeck, M., Chen, H., Van Humbeeck, J., Augustijns, P., Van den Mooter, G., Martens, J.S., 2008. Physical state of poorly water soluble therapeutic molecules loaded into SBA-15 oredered mesoporous silica carriers: a case study with itraconazole and ibuprofen. Langmuir 24, 8651–8659.
Nanubolu, J.B., Burley, J.C., 2012. Investigating the recrystallization behavior of amorphous paracetamol by variable temperature Raman studies and surface Raman mapping. Mol. Pharm. 9, 1544–1558.
Paudel, A., Raijada, D., Rantanen, J., 2015. Raman spectroscopy in pharmaceutical product design. Adv. Drug Deliv. Rev. 89, 3–20.
Pellow-Jarman, M.V., Hendra, P.J., Lehnet, R.J., 1996. The dependence of Raman signal intensity on particle size for crystal powders. Vib. Spectrosc. 12, 257–261.
Priemel, P.A., Grohganz, H., Gordon, K.C., Rades, T., Strachan, C.J., 2012. The impact of surface- and nano-crystallisation on the detected amorphous content and the dissolution behavior of amorphous indomethacin. Eur. J. Pharm. Biopharm. 82, 187–193.
Priemel, P.A., Laitinen, R., Barthold, S., Grohganz, H., Lehto, V.-P., Rades, T., Strachan, C.J., 2013. Inhibition of surface crystallization of amorphous indomethacin particles in physical drug-polymer mixtures. Int. J. Pharm. 456, 301–306.
Riikonen, J., Mäkilä, E., Salonen, J., Lehto, V.-P., 2009. Determination of the physical state of drug molecules in mesoporous silicon with different surface chemistries. Langmuir 25 (11), 6137–6142.
Rinnan, Å., van der Berg, F., Engelsen, S.B., 2009. Review of the most common pre-processing techniques for near-infrared spectra. Trends Anal. Chem. 28 (10), 1201–1222.
Savolainen, M., Jouppila, K., Pajamo, O., Christiansen, L., Strachan, C., Karjalainen, M., Rantanen, J., 2007. Determination of amorphous content in the pharmaceutical process environment. J. Pharm. Pharmacol. 59, 161–170.
Savolainen, M., Kogermann, K., Heinz, A., Aaltonen, J., Peltonen, L., Strachan, C., Yliruusi, J., 2009. Better understanding of dissolution behavior of amorphous drugs by *in-situ* solid-state analysis using Raman spectroscopy. Eur. J. Pharm. Biopharm. 741, 71–79.
Strachan, C.J., Rades, T., Gorden, K., Rantanen, J., 2007. Raman spectroscopy for quantitative analysis of pharmaceutical solids. J. Pharm. Pharmacol. 59, 179–192.
Takeuchi, H., Nagira, S., Yamamoto, H., Kawashima, Y., 2005. Solid dispersion particles of amorphous indomethacin with fine porous silica particles by using spray–drying method. Int. J. Pharm. 293, 155–164.
Talja, R.A., Roos, Y.H., 2001. Phase and state transition effects on dielectric, mechanical, and thermal properties of polyols. Thermochim. Acta 380, 109–121.
Tian, F., Zhang, F., Sandler, N., Gordon, K.C., McGoverin, C.M., Strachan, C.J., Saville, D. J., Rades, T., 2007. Influence of sample characteristics on quantification of carbamazepine hydrage formation by X-ray powder diffraction and Raman spectroscopy. Eur. J. Pharm. Biopharm. 66, 466–474.
Tripathi, P., Romanini, M., Tamarit, J.L., Macovez, R., 2015. Collective relaxation dynamics and crystallization kinetics of the amorphous Biclotymol antiseptic. Int. J. Pharm. 495 (1), 420–427.
Ueda, H., Ida, Y., Kadota, K., Tozuka, Y., 2014. Raman mapping for kinetic analysis of crystallization of amorphous drug based on distributional images. Int. J. Pharm. 462, 115–122.
Ward, S., Perkins, M., Zhang, J., Roberts, C.J., Madden, C.E., Luk, S.Y., Patel, N., Ebbens, S.J., 2005. Identifying and mapping surface amorphous domains. Pharm. Res. 22 (7), 1195–1202.
Watanabe, T., Wakiyama, N., Usui, F., Ikeda, M., Isobe, T., Senna, M., 2001. Stability of amorphous indomethacin compounded with silica. Int. J. Pharm. 226, 81–91.
Wu, T., Yu, L., 2006. Surface crystallization of indomethacin below T_g. Pharm. Res. 23 (10), 2350–2355.
Wu, T., Sun, Y., de Villiers, M.M., Yu, L., 2007. Inhibiting surface crystallization of amorphous indomethacin by nanocoating. Langmuir 23, 5148–5153.
Xu, W., Riikonen, J., Lehto, V.-P., 2013. Mesoporous systems for poorly soluble drugs. Int. J. Pharm. 453, 181–197.
Yu, L., 2016. Surface mobility of molecular glasses and its importance in physical stanility. Adv. Drug. Deliv. Rev.. http://dx.doi.org/10.1016/j.addr.2016.01.005.
Yu, L., 2001. Amorphous pharmaceutical solids: preparation: characterization and stabilization. Adv. Drug Deliv. Rev. 28, 27–42.
Zhu, L., Jona, J., Nagapudi, K., Wu, T., 2010. Fast surface crystallization of amorphous griseofulvin below T_g. Pharm. Res. 27, 1558–1567.
Zhu, L., Wong, L., Yu, L., 2008. Surface-Enhanced crystallization of amorphous nifedipine. Mol. Pharm. 5 (6), 921–926.